Journal of Naval Architecture and Marine Engineering
June, 2022
https://doi.org/10.3329/jname.v19i1.55052 *http://www.banglajol.info*

COMBINED CONVECTIVE AND VISCOUS DISSIPATION EFFECTS ON PERISTALTIC FLOW OF ELLIS FLUID IN A NON-UNIFORM TUBE

M. M. Channakote[1*], D. V. Kalse[2]

[1*]Department of Mathematics and Statistics, M. S. Ramaiah University of Applied Science, Bengaluru, Karnataka 560054, India, mchannakote@rediffmail.com

[2]Department of Mathematics, Gurunanak Dev Engineering College, Bidar, Mailoor Road Bidar, Karanataka 585403, India, kalsedilip@gmail.com

Abstract:

This paper investigates the peristaltic transport of Ellis fluid in a non-uniform tube with combined effects of convective and viscous dissipation analytically. Mathematical modeling is carried out by utilizing long wavelength and low Reynolds number assumptions. Analysis of wall properties is also included. The expressions for velocity, temperature profile, and stream function are obtained subjected to convective boundary conditions. The peristaltic transport significant characteristics are delineated with plots for various Ellis fluid parameter values. The higher rigidity and stiffness values increased the number of streamlines due to liquid circulation in the shear-thinning example, whereas the viscous damping force parameter had the reverse trend.

Keywords: Peristaltic transport, Ellis fluid, convective boundary condition, viscous dissipation, non-uniform tube.

1. Introduction

Peristalsis is a protuberant mechanism that pushes material forward in a tube or channel bypassing fluid through an effecting contractile circle over the tube. Peristaltic motion problems are commonly used in channel/tube processes in both physiology and engineering. Swallowing food through the esophagus, the evolution of chyme in the gastrointestinal tract, ovum movement in the female fallopian tube, vasomotion of small blood vessels, urine transit from the kidney to the bladder, spermatozoa transit in the efferent ducts of the male reproductive tract. The industrial applications of peristalsis include corrosive fluid transportation and sanitary fluid carriage.

The association between shear stress and shear rate in non-Newtonian fluids is nonlinear. In recent years, non-Newtonian fluids have become nearly indispensable in medical science, chemical products, and technology. As a result, a non-Newtonian fluid in a system has become increasingly popular. The Williamson fluid model, the Casson fluid model, the power-law fluid model, the Prandtl model, the Jeffrey fluid model, the Powell-Eyring fluid model, the Rabinowitsch fluid model, and the Ellis fluid model were all presented considering the importance of the flow regime aspects of non-Newtonian fluids. The classical work of Raju and Devanathan (1972) initiated a framework to study the non-Newtonian fluids by considering the power-law model. Motivated by this, numerous researchers have worked in this direction. The important studies of recent years comprise (Nagarani and Lewis, 2012, Rathod and Mahadev, 2012, Vajarvelu et al. 2013, Sankad and Asha Patil. 2016, Ebaid et al. 2017, Devaki et al., 2018, Hayat et al. 2019, Hina Sadaf and Nadeem, 2017, Mahadev et al. 2022).

Many complex processes are involved in heat transmissions, such as analyzing skin injuries, destroying undesired cancer tissues, using a dilution approach to examine blood flow, hemodialysis processes, oxygenation, drug delivery systems, manufacturing paper, vasodilation, food processing, metabolic heat generation, and radiation between a surface and its surroundings. Blood flow may be increased when a man engages in arduous physical activity or when the body is exposed to and highly hot environment. To accommodate the increased blood flow, the artery's diameters must be suitably enlarged. When the temperature of the atmosphere exceeds 20°C, heat transfer comes from the surface of the skin by dissipation through perspiration, and when the temperature is less than 20°C, heat in the human body declines via both conduction and radiation.

1813-8535 (Print), 2070-8998 (Online) Received on: Aug., 2021

In the last few decades, the literature on peristalsis with heat transfer is considerable, and several studies on this approach may be consulted. (Nadeem et al. 2014, 2014, Akram et al. 2020, 2020, Akbar et al. 2021). Channakote et al., (2021) addressed the heat transfer influence on the peristaltic flow of Rabinowitsch fluid in a conduit with porous walls. Vajravelu et al. (2011) reported the interaction of heat transfer on the peristaltic transport of a Jeffrey fluid in a vertical porous stratum. Rathod et al. (2014) discussed the peristaltic pumping of fractional second-grade fluid with heat transfer in a cylindrical tube. Wahed et al. (2019) studied the MHD peristaltic flow of Jeffery fluid with the Joule heat effect using the multi-step differential transform method. Asha et al. (2019) addressed the peristalsis with a combined effect of hall and heat transfer on the MHD flow of Jeffrey fluid in an asymmetric vertical porous channel. Rafiq and Abbas (2021) reported the effects of viscous dissipation and heat radiation on the Rabinowitsch fluid model with wall characteristics that obey the peristaltic process.

The Ellis fluid model is one of the fluid models in which the shear stress and shear rate have a nonlinear relationship. The generalization of power-law and Bingham (viscoelastic) models is the Ellis model. Furthermore, the study of Ellis fluid model is a well-established model for describing the non-Newtonian nature of the fluid, and also it is used in the study to calculate the flow characteristics of peristaltic transport in the channel/tube. Ellis fluid has the advantage of being able to predict Newtonian behavior at low shear stresses and power-law behavior at high shear stresses. Ellis fluid and power-law connections are prominent constitutive equations for representing non-Newtonian fluids' shear-thinning behavior. This aspect of the Ellis fluid model allows it to accurately depict the rheological properties of much polymeric fluid divergent. The application of these fluid models is very useful in predicting the rheology of several bio-fluids such as blood, cervical mucus, respiratory mucus, chime, etc.

Ali et al. (2015) studied the peristaltic pumping of Ellis fluid in a channel. Abbas et al. (2017) investigated the peristaltic blood flow of Ellis fluid in a non-uniform channel with a complaints wall. Kumar et al. (2018) studied the peristaltic motion of an Ellis fluid model in an inclined tube with wall properties. Ali et al. (2019) addressed the mathematical modeling of two-fluid electro-osmotic peristaltic pumping in an axisymmetric tube with an Ellis fluid. Saravana et al. (2020) looked at the effects of complete slip-on peristaltic transport of Ellis fluid through a flexible tube.

Because of the above studies, one can perceive that no examination of the combined convective and viscous dissipation effects on peristaltic flow of Ellis fluid in a cylindrical tube with wall properties has been present in the available literature. With the aforementioned motive in mind, we intended to investigate the effects of viscous dissipation on the peristaltic transport of the Ellis fluid model in a non-uniform vertical tube. The energy equation takes into consideration the convective slip effect. To simplify the normalized constitutive equations, a long-wavelength and low Reynolds number approximation are adopted. The effects of relevant attention parameters on velocity, temperature, and streamlines for Ellis fluid prototypes are commonly encountered and deliberated using graphs. The current study qualitatively depicts the biofluid rheology of a complicated flow through a tube with a muscle wall, and it has a wide variety of applications for describing blood flow dynamics in vessels while assuming the necessary wall properties. The research also predicts physiological flow characteristics (namely blood flow) in a tube/channel with the (muscular) wall.

2. Mathematical Formulation

Consider the peristalsis of Ellis fluid in a non-uniform tube in the presence of a compliant wall for the two-dimensional flow of an incompressible fluid. The geometry of the problem is shown in fig. 1.

The mass, momentum, and energy conservation equations can be described as:

$$\frac{1}{r^*}\frac{\partial(r^* u^*)}{\partial r^*} + \frac{\partial w^*}{\partial z^*} = 0 \,, \tag{1}$$

$$\rho\left(\frac{\partial u^*}{\partial t^*} + u^*\frac{\partial u^*}{\partial r^*} + w^*\frac{\partial u^*}{\partial z^*}\right) = -\frac{\partial p^*}{\partial r^*} + \frac{1}{r^*}\frac{\partial(\tau_{11}^*)}{\partial r^*} + \frac{\partial \tau_{13}{}^*}{\partial z^*} - \frac{\tau_{22}{}^*}{r^*}, \tag{2}$$

$$\rho\left(\frac{\partial w^*}{\partial t^*}+u^*\frac{\partial w^*}{\partial r^*}+w^*\frac{\partial w^*}{\partial z^*}\right)=-\frac{\partial p^*}{\partial z^*}+\frac{1}{r^*}\frac{\partial(r^*\tau^*_{13})}{\partial r^*}+\frac{\partial \tau_{33}{}^*}{\partial z^*}, \tag{3}$$

$$\rho c_p\left(\frac{\partial T^*}{\partial t^*}+u^*\frac{\partial T^*}{\partial r^*}+w^*\frac{\partial T^*}{\partial z^*}\right)=k_1\left(\frac{\partial^2 T^*}{\partial r^{*2}}+\frac{1}{r^*}\frac{\partial T^*}{\partial r^*}+\frac{\partial^2 T^*}{\partial z^{*2}}\right)$$
$$+\tau^*_{11}\frac{\partial u^*}{\partial r^*}+\tau^*_{33}\frac{\partial u^*}{\partial z^*}+\tau_{13}\left(\frac{\partial w^*}{\partial r^*}+\frac{\partial u^*}{\partial z^*}\right). \tag{4}$$

In the transverse coordinates, u^* and w^* are the velocity components, respectively, ρ is density, p is pressure, T^* is temperature, k_1 is thermal conductivity, c_p is specific heat, t^* is the time, $\tau_{11},\tau_{13},\tau_{33},\tau_{12}$ are stress tensor components.

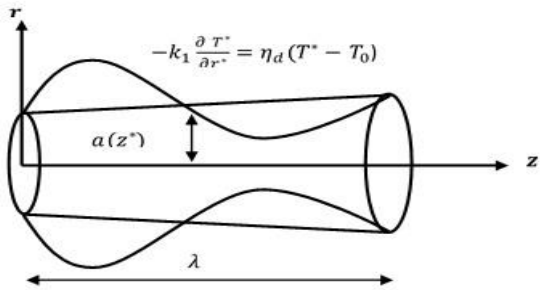

Fig. 1: The geometry of the problem

The useful boundary conditions for the study concern problem are:

$$w^*=0,\ \ at\ \ H^*=a(z^*)+b\sin\frac{2\pi}{\lambda}\left(z^*-ct^*\right), \tag{5}$$
$$\frac{\partial w^*}{\partial r^*}=0\,,\quad at\quad r^*=0\,,$$

where H^* is the non-uniform wave in which $a(z^*)$ is the non-uniform radius, and b is the wave amplitude.

$$-k\frac{\partial \Gamma^*}{\partial r^*}=\eta_d\left(T^*-T_0\right)\ at\ r^*=H^*,\frac{\partial T^*}{\partial r^*}=0,\ at\ r^*=0\,. \tag{6}$$

We introduce the following non-dimensional parameters:

$$\left.\begin{aligned} &w=\frac{w^*}{c}, u=\frac{u^*}{c\delta}, z=\frac{z^*}{\lambda}, r=\frac{r^*}{a_2}, \delta=\frac{a_2}{\lambda}, p=\frac{p\,a_2^2}{c\lambda\mu}, R_e=\frac{\rho\,c\,a_2^2}{\mu}, \theta=\frac{T^*-T_0}{T_0}, t=\frac{c\,t^*}{\lambda}\\ &pr=\frac{\mu\,c_p}{k_1}, Ec=\frac{c^2}{T_0\,c_p}., \phi=\frac{b}{a_2}, \tau_{i,j}=\frac{a_2\,\tau^*_{i,j}}{c\,\mu}, E_1=-\frac{\sigma\,a_2^3}{\lambda^3\mu\,c}, E_2=-\frac{m\,a_2^3}{\lambda^3\mu}, \kappa=\frac{a_2\eta_d}{k_1}\\ &E_3=-\frac{c\,a_2^3}{\lambda^2\mu}, a(z^*)=a_2+k\,z^*, h=\frac{H^*}{a_2}=1+\frac{\lambda\,k\,z}{a_2}+\phi\sin 2\pi(z-ct), Br=Ecpr, \end{aligned}\right\} \quad (7)$$

where δ is the wavenumber, ϕ is the amplitude ratio, Ec is the Eckert number, and pr is the Prandtl number respectively. With the help of Eq. (7) and under the conditions of long wavelength and low Reynolds number, equations. (1)- (6) taking the following form:

$$\frac{1}{r}\frac{\partial(r\,u)}{\partial\,r}+\frac{\partial\,w}{\partial\,z}=0\ , \quad (8)$$

$$\frac{\partial p}{\partial r}=0, \quad (9)$$

$$\frac{\partial p}{\partial z}=\frac{1}{r}\frac{\partial\left(r\tau_{13}\right)}{\partial\,r}, \quad (10)$$

$$\left[\frac{1}{r}\frac{\partial\theta}{\partial\,r}+\frac{\partial^2\theta}{\partial\,r^2}\right]=-Br\tau_{13}\left(\frac{\partial\,w}{\partial\,r}\right). \quad (11)$$

The governing equation of motion of flexible walls may be quantified (Kumar et al. 2013, Srinivas et al. 2009).

$$L(H^*)=p^*-p_0\,. \quad (12)$$

The operator characterizes the motion of the stretched membrane, such that

$$L=-\sigma\frac{\partial^2}{\partial\,z^{*2}}+m\frac{\partial^2}{\partial\,t^{*2}}+C'\frac{\partial}{\partial\,t^*} \quad (13)$$

Furthermore, we infer that $p_0=0$ since p_0 reflects the pressure exerted on the outside of the wall's surface due to muscle tension. After dimensionless it becomes

$$\frac{\partial p}{\partial z}=\frac{\partial\,L(h)}{\partial\,z}=E_1\frac{\partial^3 h}{\partial z^3}+E_2\frac{\partial^3 h}{\partial z\,\partial t^2}+E_3\frac{\partial^2 h}{\partial z\,\partial t}=A(z,t)\,. \quad (14)$$

The component of τ_{13} is attained by making use of Eq. (10) in the stress tensor specified in Refs. Ali et al. 2019 and Sarvana et al. 2020).

$$\frac{\partial w}{\partial r}=\tau_{13}+\eta\left|(\tau_{13})\right|^{n-1}\tau_{13}\,. \quad (15)$$

The non-dimensional form of the boundary conditions is

$$\frac{\partial w}{\partial r}=0\ \ at\ \ r=0, w=0\ \ at\ \ r=h\,. \quad (16)$$

$$\frac{\partial \theta}{\partial t} + \kappa\, \theta = 0 \;\; at \;\; r = h, \;\; \frac{\partial \theta}{\partial r} = 0 \;\; at \;\; r = 0 . \tag{17}$$

Longitudinal momentum Eq. (10) subjected to the boundary condition $\tau_{13} = 0$ at the symmetry line $r = 0$ yield

$$\tau_{13} = \frac{r}{2}\frac{\partial p}{\partial z} = A(z,t). \tag{18}$$

3. Solution Procedure

The exact solution of Eqs. (11) and (15) by imposing the boundary conditions Eq. (16) and Eq. (17) are obtained as:

$$w = \left(r^2 - h^2\right)\frac{A}{4} + \left(r^{n+1} - h^{n+1}\right)\frac{A^n\, \eta}{2^n\, (n+1)} \tag{19}$$

$$\theta = \frac{BrA^2}{64} + \left(h^4 - r^4\right) + Br\left(h^{n+3} - r^{n+3}\right)\frac{A^{n+1}\, \eta}{2^n\, (n+3)^2} + \frac{Br}{\kappa}\left(\frac{h^2 A^2}{16} + \frac{h^{n+2} A^{n+1} \eta}{2^{n+1}(n+3)}\right) \tag{20}$$

The corresponding stream function can be obtained by using the formula

$$u = -\frac{1}{r}\frac{\partial \psi}{\partial r}, \;\; w = \frac{1}{r}\frac{\partial \psi}{\partial r} \; at \;\; r = h . \tag{21}$$

Where,

$$A(z,t) = \phi\left(-(2\pi)^3\right)\cos\left[2\pi(z-ct)\right]\left(E_1 + E_2\right) + E_3(2\pi)^2 \sin\left[2\pi(z-ct)\right]. \tag{22}$$

4. Results and Discussion

The major goal of this study is to look into the peristaltic flow of Ellis fluid in a cylindrical tube with wall properties. The convective slip effect is taken into account in the energy equation. As a result, this section will explore the impact of various parameters on the axial velocity w and temperature θ. The results of pseudo plastic, dilatant, and Newtonian fluids, as well as other parameters, are briefly discussed. Furthermore, streamlined graphs are used to highlight the trapping phenomenon.

Figs. (2) and (3) show the deviation of the velocity profile w as the rigidity parameter E_1 and stiffness parameter E_2 are increased, respectively. For shear-thinning and viscous situations, values of E_1 and E_2 are noticeable. Because of the wall properties, less resistance is accessible to the flow, and thus velocity increases; however, the reverse behavior is represented in the case of shear thickening. Furthermore, in the case of shear thinning, the velocity profile has a bigger curve, but the curve for viscous fluid has a smaller variation. Fig. 4 illustrates the velocity profiles for the viscous damping force parameter E_3. For increasing E_3 values, the velocity curve gets smaller deviations and decreases for increasing values of dilatant but has the opposite behavior for pseudo-plastic and viscous fluids.

Fig. 5 and 6 show the influence of different parameters on temperature. Fig. 5 shows that as the Brinkman number Br rises, the temperature profile is an increasing function for a pseudo plastic, dilatant, and Newtonian fluid. Higher Br values, in general, suggest greater viscous dissipation, or more heat generation due to resistance in the flow induced by shear, which increases the fluid temperature.

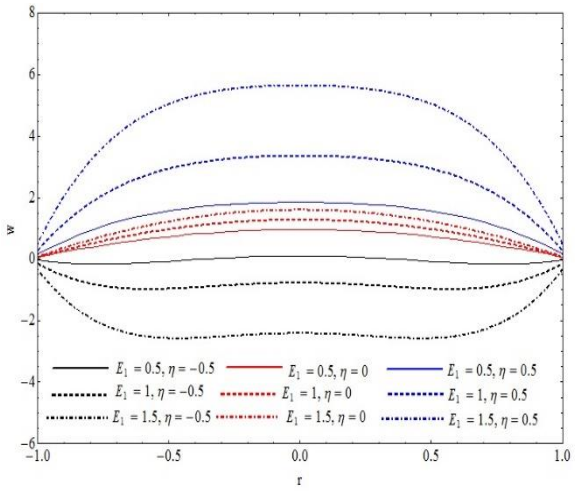

Fig.2: Velocity profile for various values of E_1, η at $E_2 = 1, . \mathrm{E}_3 = 0.5, \phi = 0.01, \lambda = 0.02. \kappa = 0.24,$ $t = 0.025, l = 0.34, n = 3$

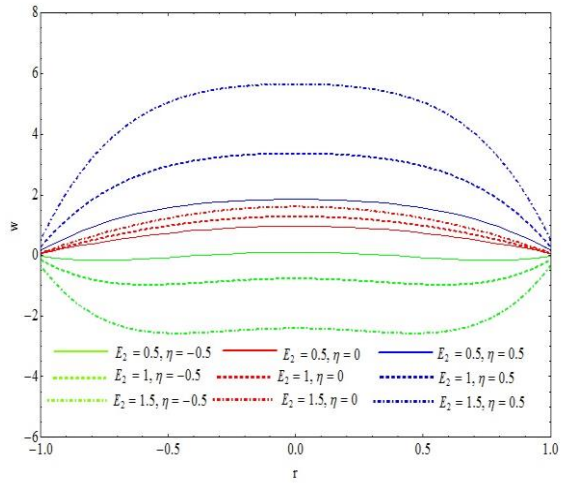

Fig.3: Velocity profile for various values of E_2, η at $E_1 = 1, . \mathrm{E}_3 = 0.5, \phi = 0.01, \lambda = 0.02, . \kappa = 0.24,$ $t = 0.025, l = 0.34, n = 3$

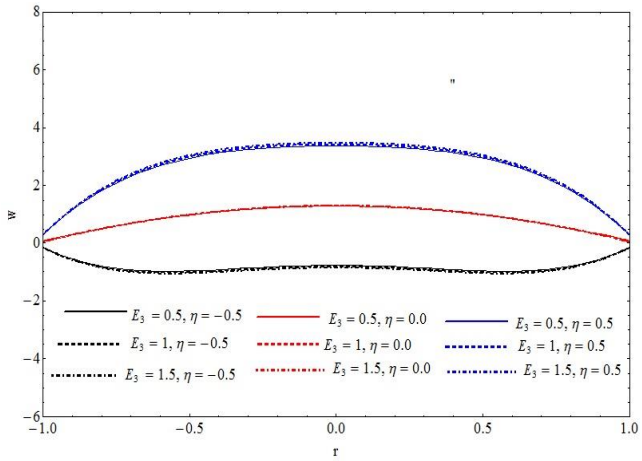

Fig.4: Velocity profile for various values of E_3, η $E_1 = 1, E_2 = 0.5, \phi = 0.01, \lambda = 0.02, \kappa = 0.24, , t = 0.025, l = 0.34, n = 3.$

Fig. 6 shows the temperature profile for varying Biot number values. As the dimensionless Biot number κ is increased, the temperature profile for all three cases decreases (Pseudo plastic, dilatant, and viscoelastic fluid). The reason for this is that as the κ increases, the thermal conductivity declines, leading to a reduction in the temperature profile.

The temperature profile for the elasticity parameter is graphically depicted in Figs. 7-9. For all rising values of rigidity parameter E_1, stiffness parameter E_2, and viscous fluid E_3, the temperature profile increases. In the dilatant (pseudo plastic) case, variations for the damping force parameter are also similar. Variations in the damping force are also closer in the case of pseudo plastic.

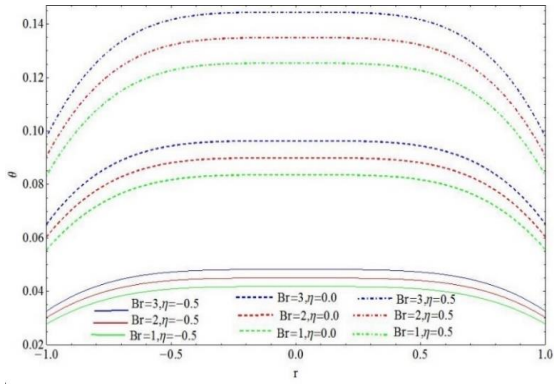

Fig.5: Temperature profile for various values of Br, η at $E_1 = 1, E_2 = 1, E_3 = 0.5, t = 0.025, l = 0.24, n = 2$ $k = 2.4,\ z = 0.02, Br = 2, \phi = 0.01, \lambda = 0.07$

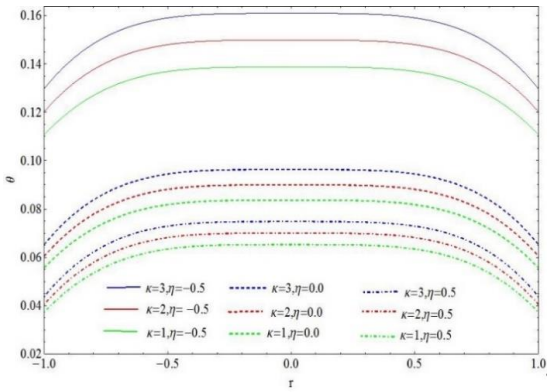

Fig.6: Temperature profile for various values of κ, η at $E_1 = 1.5, E_3 = 0.5, \phi = 0.01,$ $\lambda = 0.07, k = 2.4, \kappa = 2, l = 0.24, Br = 2$

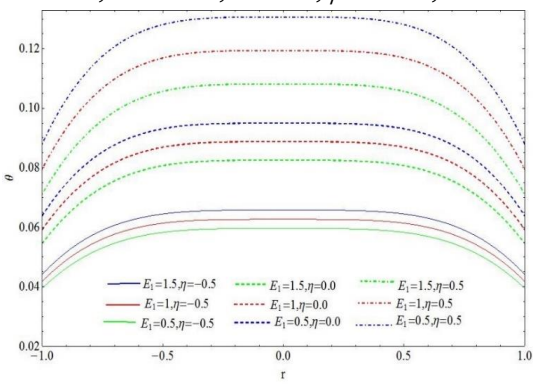

Fig. 7: Temperature profile for various values of E_1, η at $Br = 2, E_2 = 1, E_3 = 0.5, t = 0.25, l = 0.24, n = 2$ $k = 2.4,\ z = 0.02, Br = 2, \phi = 0.01, \lambda = 0.07, \kappa = 2$

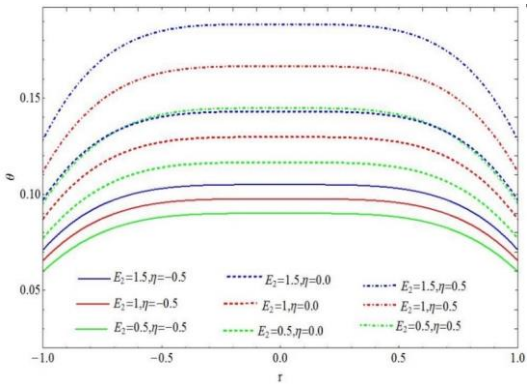

Fig. 8: Temperature profile for various values of E_2, η at $E_1 = 1.5, E_3 = 0.5, \phi = 0.01,$ $\lambda = 0.07, k = 2.4, \kappa = 2, l = 0.24, Br = 2$

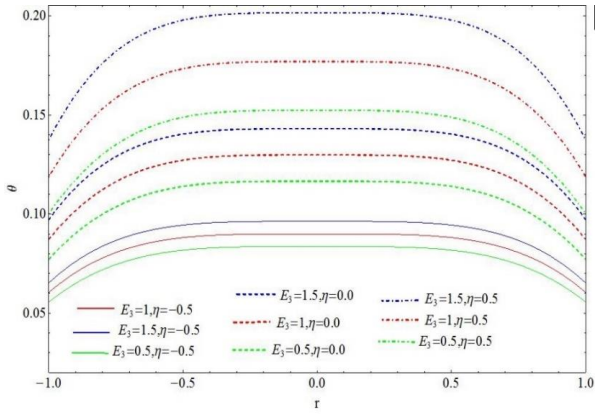

Fig. 9: Temperature profile for various values of E_3, η at $E_1 = 0.5, E_1 = 0.5, \phi = 0.01, \lambda = 0.02, \kappa = 0.24, t = 0.025, l = 0.34, n = 3,\ Br = 2.$

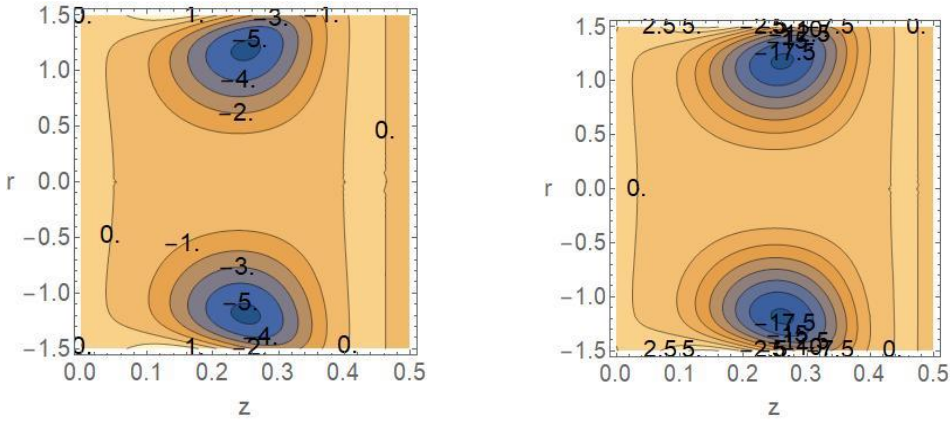

$(a)\ \ E_1 = 0.5, \eta = -0.5$ $(b)\ \ E_1 = 1, \eta = -0.5$

Fig.10: Streamlines for $\phi = 0.03,\ \lambda = 0.07, l = 0.22, n = 3, t = 0.25, E_1 = 0.5, E_3 = 1.5, k = 2.4$.

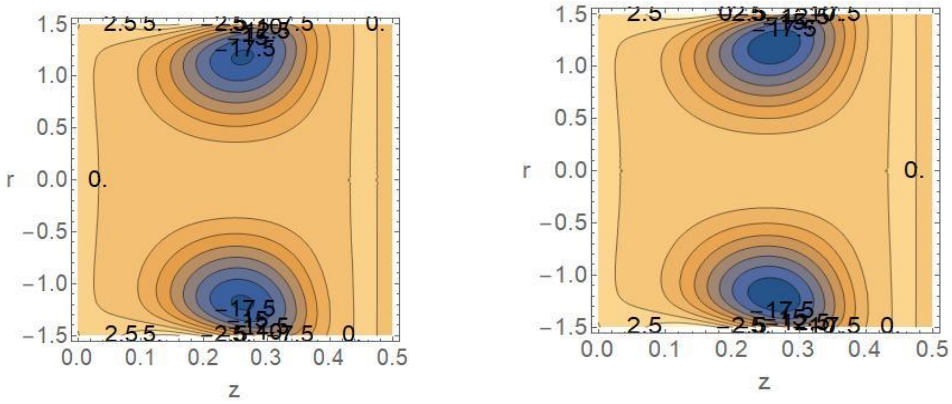

$(a)\ \ E_2 = 0.5, \eta = -0.5$ $(b)\ \ E_2 = 1, \eta = -0.5$

Fig.11: Streamlines for $\phi = 0.03,\ \lambda = 0.07, l = 0.22, n = 3, t = 0.25, E_1 = 0.5, E_3 = 1.5, k = 2.4$.

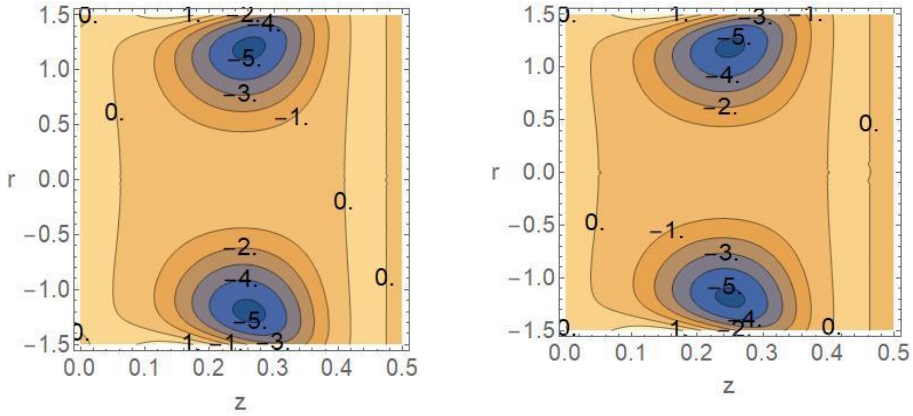

$(a)\ \ E_3 = 0.5,\ \eta = -0.5$ $(b)\ \ E_3 = 1,\ \eta = -0.5$

Fig.12: Streamlines for $\phi = 0.03,\ \lambda = 0.07, l = 0.22, n = 3, t = 0.25, E_1 = 0.5, E_2 = 1.5, k = 2.4$.

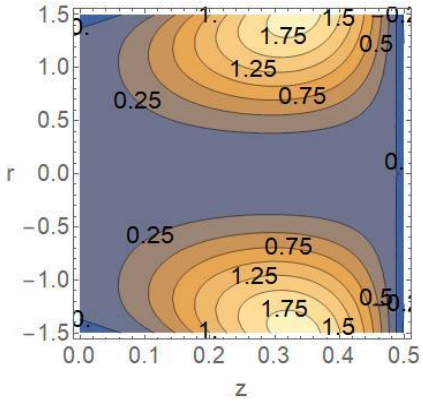

(a) $E_1 = 0.5, \eta = 0$

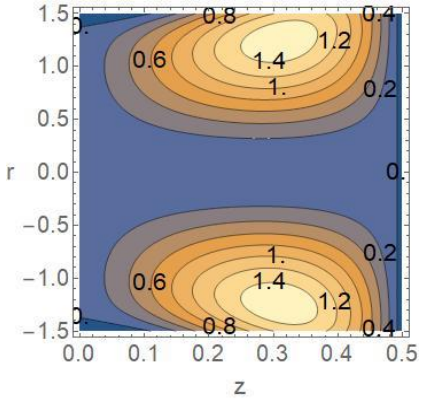

(b) $E_1 = 1, \eta = 0$

Fig.13: Streamlines for $\phi = 0.03,\ \lambda = 0.07, l = 0.22, n = 3, t = 0.25, E_2 = 0.5, E_3 = 1.5, k = 2.4$ ..

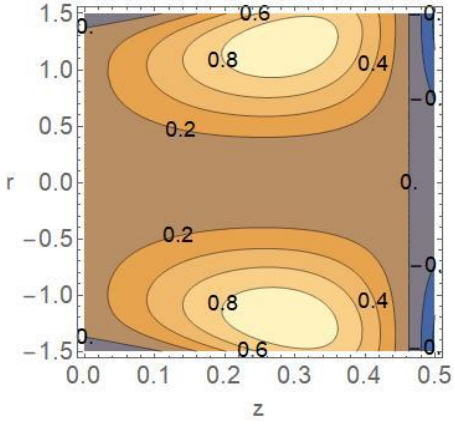

(a) $E_2 = 0.5, \eta = 0$

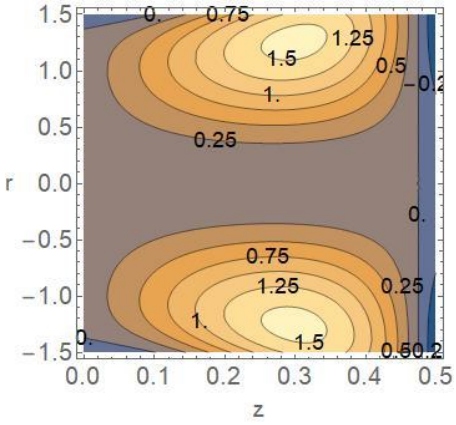

(b) $E_2 = 1, \eta = 0$

Fig.14: Streamlines for $\phi = 0.03,\ \lambda = 0.07, l = 0.22, n = 3, t = 0.25, E_1 = 0.5, E_3 = 1.5, k = 2.4$.

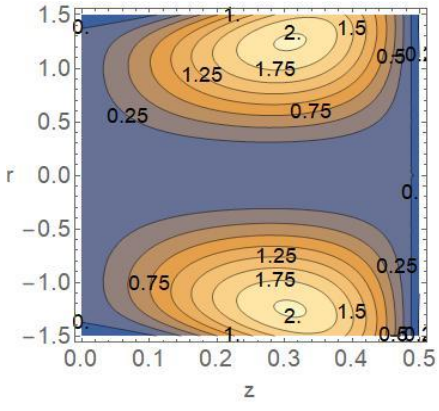

(a) $E_3 = 1, \eta = 0$

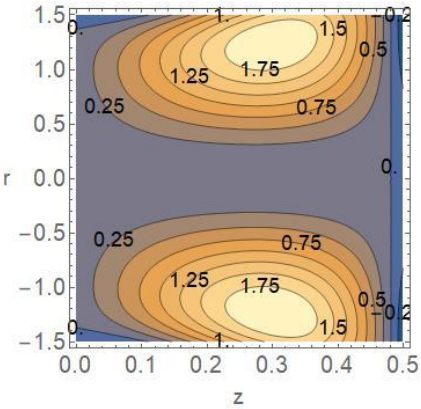

(b) $E_3 = 1.5, \eta = 0$

Fig.15: Streamlines for $\phi = 0.03,\ \lambda = 0.07, l = 0.22, n = 3, t = 0.25, E_1 = 0.5, E_2 = 1.5, k = 2.4$.

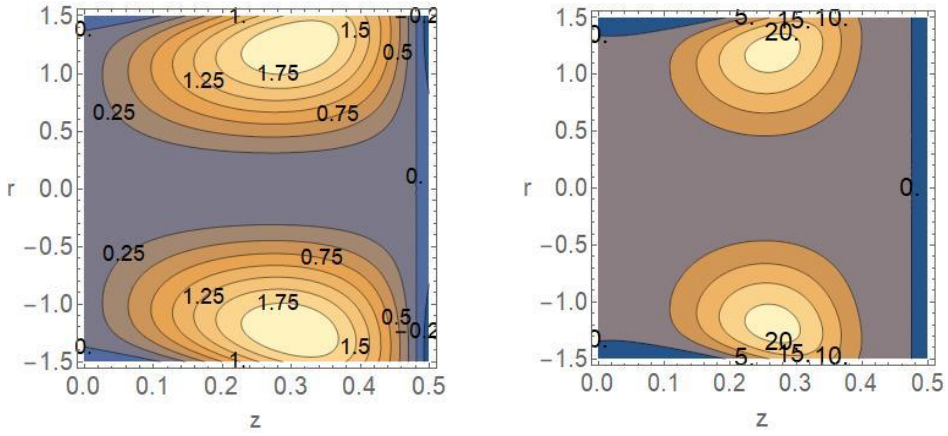

$(a)\ E_1 = 0.5, \eta = 0.5$ $(b)\ E_1 = 1, \eta = 0.5$

Fig.16: Streamlines for $\phi = 0.03,\ \lambda = 0.07, l = 0.22, n = 3, t = 0.25, E_2 = 0.5, E_3 = 1.5, k = 2.4$.

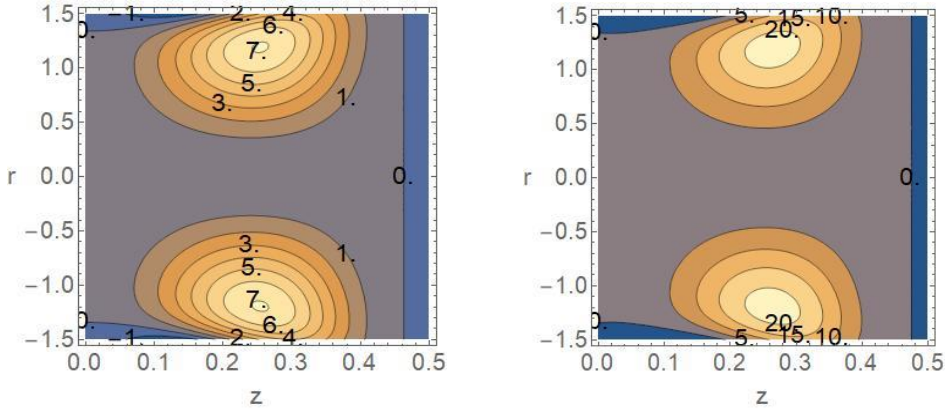

$(a)\ E_2 = 0.5, \eta = 0.5$ $(b)\ E_2 = 1, \eta = 0.5$

Fig.17: Streamlines for $\phi = 0.03,\ \lambda = 0.07, l = 0.22, n = 3, t = 0.25, E_1 = 0.5, E_3 = 1.5, k = 2.4$.

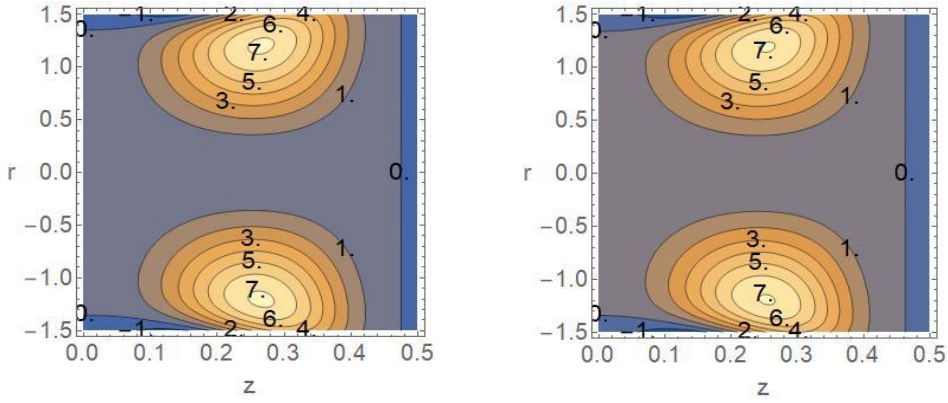

$(a)\ E_3 = 1, \eta = 0.5$ $(b)\ E_3 = 1.5, \eta = 0.5$

Fig.18: Streamlines for $\phi = 0.03,\ \lambda = 0.07, l = 0.22, n = 3, t = 0.25, E_1 =, E_2 = 0.5, k = 2.4$.

5. Conclusion

The impact of viscous dissipation and convective analysis on the peristaltic transport of the Ellis fluid model in a non-uniform tube is investigated in this research. Analytical solutions are obtained for the velocity and temperature profile. The flow behavior is investigated using graphs. The most significant findings are summarized here.

- For pseudo-plastic and viscous liquids, the elastic nature of the walls delivers less resistance to flow, and increasing rigidity parameter E_1, stiffness parameter E_2, and viscous damping force parameter E_3 rises the velocity profile, but for dilatant liquids, the opposite conduct is depicted.
- The velocity profile is found to be an increasing function of the rigidity parameter, stiffness parameter, and viscous damping force parameter for shear-thinning and viscous fluids due to the lower resistance given by the walls, whereas the reverse trend is observed for shear thickening fluids.
- For shear thinning, shear thickening, and viscous fluid, the temperature profile is increasing as the Brinkman number increases. A physically larger value of Br fluid temperature rises because shear in the flow generates more heat due to friction, raising the fluid temperature.
- The temperature profile declines as the Biot number increases.
- The trapping bolus width increases as the rigidity and stiffness parameters for the shear thickness scenario of fluid increase. For a viscous fluid, the trapping bolus size rises somewhat, but the quantity of trapped bolus remains constant.
- The Brinkman number is known to connect with the effects of viscous dissipation, and so it aids in rising the liquid temperature in all scenarios.

References

Abbas, A.M., Bhatti, M.M. and Rashidi, M.M. (2017): Peristaltic blood flow of Ellis fluid through a non-uniform channel having compliant walls, Journal of Nanofluid, Vol. 6, No. 2, pp. 318-323. https://doi.org/10.1166/jon.2017.1314.

Ali, N., Abbasi, A., and Ahmad, I. (2015): Channel flow of Ellis fluid due to peristalsis, AIP Advances, Vol. 5, No. 9, pp. 1-9. https://doi.org/10.1063/1.4932042.

Ali, N., Hussain, S., Ullah, K., and Beg, O.A. (2019): Mathematical modeling of two-fluid electro-osmotic peristaltic pumping of an Ellis fluid in an axisymmetric tube, European Physical Journal Plus, Vol.134, No. 4, pp. 134-141,https://doi.org/10.1140/epjp/i2019-12488-2.

Asha, S. K., and Deepa, C. K. (2019): Impacts of the hall and heat transfer on peristaltic blood flow of an MHD Jeffrey fluid in a vertical asymmetric porous channel, International Journal of Advances in Applied Mathematics and Mechanics, Vol, 6. No.4, pp.55-63.

Akbar, N., S., Maraj, E.N., Akhtar, S., Ali, E. and Anqui, A., E. (2021): Heat transfer analysis of MHD viscous fluid in a ciliated tube with entropy generation, Mathematical Methods in the Applied Sciences, pp. 1-1410. https://doi.org/10.1002/mma.7906.

Akram, J., Akbar, N., S., and Maraj, E. N. (2020): Chemical reaction and heat source/sink effect on magneto nano Prandtl-Eyring fluid peristaltic propulsion in an inclined symmetric channel, Chinese Journal of Physics, Vol.65.No.pp.300-313. doi.org/10.1016/j.cjph.2020.03.004 .

Akram, J., Akbar, N., S., Maraj, E. N. (2020): A comparative study on the role of nanoparticle dispersion in electro-osmosis regulated peristaltic flow of water, Alexandria Engineering Journal, Vol. 59. No.2, pp. 943-956. https://doi.org/10.1016/j.aej.2020.03.017.

Channakote, M.M., and Dilipkumar, V.K. (2021): Heat transfer in peristaltic motion of Rabinowitsch fluid in a channel with a permeable wall, Applications Applied Mathematics, Vol, 16, pp. 1057-1076. https://digitalcommons.pvamu.edu/aam/vol16/iss2/16.

Devaki, P., Sreenadh, S., Vajravelu, K., Prasad, K.V., and Hanumesh, V. (2018): Wall properties and slip consequences on peristaltic transport of Casson liquid in a flexible channel with heat transfer, Applied Mathematical and Nonlinear Sciences, Vol.3. No.1, pp.277-290. https://doi.org/10.21042/AMNS.2018.1.00021.

Ebaid, A., Aly, E. H., and Vajravelu, K. (2017): Analytical solution for peristaltic transport of viscous nanofluid in an asymmetric channel with full slip and convective conditions, Communications in Theoretical Physics, Vol.68, No.3, pp. 96–102.https://doi.org/10. 1088/0253-6102/68/1/9/96.

Hasona, W.M., El-shekhipy, A.A., and Ibrahim, M.G. (2019): Semi-analytical solution to MHD peristaltic flow of a Jeffrey fluid in presence of joule heat effect by using the multi-step differential method, New Trends in Mathematical Sciences, Vol, 7, No.2, pp. 123-137. https://doi.org/10.20854/ntmsci2019351.

Hina, S. and Nadeem, S. (2017): Analysis of combined convective and viscous dissipation effects for peristaltic flow of Rabinowitsch fluid model, Journal of Bionic Engineering, Vol. 14, pp.182–190.https://doi.org/10.1016/S1672_6529(16)60389-x.

Hayat, T., Aslam, N., Khan, M. I., Khan, M. I., and Alsaedi, A. (2019): MHD peristaltic motion of Johnson–Segalman fluid in an inclined channel subject to radiative flux and convective boundary conditions, Computer Methods and Programs in Biomedicine, Vol. 180, pp.104999. https://doi.org/10.1016/j.cmpb.2019.104999.

Kumar, K. T., Kavitha, A., and Saravana, R. (2018): Peristaltic flow of an Ellis fluid model in an inclined uniform tube with wall properties, International Journal of Mechanical Engineering and Technology, Vol. 9, No. 2, pp. 15–27.

Kumar, K.A., Sreenadh, S., and Srinivas, A.N.S. (2013): Effects of wall properties and heat transfer on the peristaltic transport of a Jeffrey fluid in a channel, Advances in Applied Science Research, Vol.4, No.6, pp.159-172.

Mahadev, M. C., and Dilipkumar, V. K. (2022): The consequences of the wall properties and slip on the peristaltic motion of Jeffrey liquid in a non-uniform tube with heat transfer, International Journal of Creative Research Thoughts. Vol.10. No.2, pp.b300-b310.

Nagarani, P., and Lewis, A. (2012): Peristaltic flow of a Casson fluid in an annulus, Korea-Australia Rheology Journal, Vol. 24, No.2, pp. 1-9. https://doi.org/10.1007/s13367-012-0001-6.

Nadeem, S., and Maraj, E. N. (2014): The mathematical analysis for peristaltic flow of a Nano-fluid in a curved channel with compliant walls, Applied Nano Science, Vol, 4, No. pp.85-92.

Nadeem, S., and Maraj, E. N. (2014): Theoretical analysis for peristaltic flow of Carreau nanofluid in a curved channel with compliant walls, Journal of Computational and Theoretical, Nanoscience, Vol,11, No. 6, pp.1443-1452. https://doi.org/10.1166/jctn.2014.3516.

Raju, K. K., and Devanathan, R. (1972): Peristaltic motion of a non-Newtonian fluid, Rheological Acta. Vol.11, pp.170-178. https://doi.org/10.1007/BF01993016.

Rathod, V.P., and Mahadev, M. (2014): Interaction of heat transfer and peristaltic pumping of frictional second-grade fluid through a vertical cylindrical tube, Thermal Science, Vol. 18, No.4, pp. 1109-1118. https://doi.org/10.2298/TSCI.111022143R

Rathod, V. P., and Mahadev, M. (2012): Peristaltic flow of Jeffrey fluid with slip effect in an inclined channel, Journal of Chemical, Biological and Physical Sciences, Vol.2, pp.1987-1997.

Sankad, G.C., and Asha Patil. (2016): Impact of the permeable lining of the wall on the peristaltic flow of Herschel Bulkley fluid, Applications and Applied Mechanics (AAM), Vol. 11, No.2, pp. 663-679.

Rafiq, M. Y., and Abbas, Z. (2021): Impacts of viscous dissipation and thermal radiation on Rabinowitsch fluid model obeying peristaltic mechanism with wall properties, Arabian Journal for Science and Engineering, https://dx.doi.org/10.1007/S111369-021-05870-7.

Srinivas, S., Gayatri, R., and Kothandapani, M. (2009): The influence of slip conditions, wall properties and heat transfer on MHD Peristaltic transport. Computer Physics Communications. Vol.180, pp. 2115-2122. https://dx.doi.org/10.1016/j.cpc.2009.06.015.

Saravan, R., Sreenadh, S., Kumar P. R., and Ramesh, B. V. (2020): Peristaltic pumping of Ellis fluid through a flexible tube with complete slip effects, Journal of Naval Architecture and Marine Engineering. Vol, 17, pp.79-88. https://doi.org./10.3329/jname.v17i2.49559.

Vajravelu, K., Sreenadh, S., and Lakshmi Narayan, P. (2011): The influence of heat transfer on peristaltic transport of a Jeffrey fluid in a vertical porous stratum, Communication Nonlinear Science and Numerical Simulation, Vol,16. No. 8, pp. 3107-3125.https://dx.doi.org doi.10.1016/j.cnsns.2010.11.001.